Ultrafast Science
A SCIENCE PARTNER JOURNAL

RESEARCH ARTICLE

Ultrafast Laser Writing of Liquid Crystal Waveguides

Bohan Chen[1*†], Peng Xie[1,2,3*†], Zimo Zhao[1], Patrick S. Salter[1], Mengmeng Li[1], Linpei Xue[1], Xuke Qiu[1], Martin J. Booth[1], Steve J. Elston[1], and Stephen M. Morris[1*]

[1]Department of Engineering Science, University of Oxford, Oxford OX1 3PJ, UK. [2]Qiguang Research and Innovation Center, Aerospace Laser Technology and System Department, Shanghai Institute of Optics and Fine Mechanics, Chinese Academy of Science, Shanghai 201800, China. [3]Center of Materials Science and Optoelectronics Engineering, University of Chinese Academy of Sciences, Beijing 100049, China.

*Address correspondence to: bohan.chen2@eng.ox.ac.uk (B.C.); pengx@siom.ac.cn (P.X.); stephen.morris@eng.ox.ac.uk (S.M.M.)
†These authors contributed equally to this work.

Citation: Chen B, Xie P, Zhao Z, Salter PS, Li M, Xue L, Qiu X, Booth MJ, Elston SJ, Morris SM. Ultrafast Laser Writing of Liquid Crystal Waveguides. *Ultrafast Sci.* 2024;4:Article 0065. https://doi.org/10.34133/ultrafastscience.0065

Submitted 13 December 2023
Accepted 28 May 2024
Published 24 July 2024

With the development of conformable photonic platforms, particularly those that could be interfaced with the human body or integrated into wearable technology, there is an ever-increasing need for mechanically flexible optical photonic elements in soft materials. Here, we realize mechanically flexible liquid crystal (LC) waveguides using a combination of ultrafast direct laser writing and ultraviolet (UV) photo-polymerization. Results are presented that demonstrate that these laser-written waveguides can be either electrically switchable (by omitting the bulk UV polymerization step) or mechanically flexible. Characteristics of the waveguide are investigated for different fabrication conditions and geometrical configurations, including the dimensions of the waveguide and laser writing power. Our findings reveal that smaller waveguide geometries result in reduced intensity attenuation. Specifically, for a 10-μm-wide laser-written channel in a 14-μm-thick LC layer, a loss factor of −1.8 dB/mm at $\lambda = 650$ nm was observed. Following the UV polymerization step and subsequent delamination of the glass substrates, we demonstrate a free-standing flexible LC waveguide, which retains waveguide functionality even when bent, making it potentially suitable for on-skin sensors and other photonic devices that could interface with the human body. For the flexible LC waveguides fabricated in this study, the loss in a straight waveguide with a cross-sectional area of 20 μm × 20 μm was recorded to be −0.2 dB/mm. These results highlight the promising potential of electrically responsive and mechanically moldable optical waveguides using laser writing and UV-assisted polymer network formation.

Introduction

Fabrication technologies such as lithography [1], inkjet printing [2,3], electrohydrodynamic printing [4,5], 3-dimensional printing [6,7], and direct laser writing [8–10] have enabled the realization of micro- and nano-scale photonic devices and systems. Such photonic elements have demonstrated considerable potential in various fields including optical computing [11–19], optical communications [20–24], and optical sensing [25]. Optical waveguides can play a vital role in terms of confining and guiding light along predetermined paths, especially for photonic integrated circuits (PICs), which utilize photons for computation, akin to the function of an electric circuit in conventional microchips [15,26–32].

In general, silicon, silicon nitride, III–V semiconductors, and $LiNbO_3$ are popular material platforms for optical waveguides [33–35], which require a refractive index mismatch between the waveguide core material and its surrounding cladding. Although silicon photonic technologies have attracted significant interest in recent years and have shown revolutionary potential, they suffer from significant insertion loss due to their high refractive indices and typically do not offer switchable functionality [36,37]. While $LiNbO_3$ does exhibit outstanding electro-optical tunability, the high voltage requirements can restrict its integration into PICs [30].

Nematic liquid crystals (LCs) are potentially desirable for optical waveguides/light pipes because the refractive index can be "tuned" using a range of external stimuli [38–44]. For example, an LC splitter for generating and separating autofocusing and autodefocusing circular Airy beams was demonstrated in 2020 in which the energy distribution could be controlled by the incident polarization [45]. Recent work also demonstrated thermomechanical LC elastomers that constitute artificial muscle-like actuators that can be remotely and repeatably controlled for

large stoke and fast response [46]. Additionally, LCs also exhibit a birefringence that can be controlled by the application of a voltage, enabling a refractive index mismatch to be obtained without changing the material as is often required [47–51]. For example, recent work has demonstrated the formation of polymer-stabilized microlens arrays that can be tuned electronically and reversibly at room temperature [47].

The use of LCs in waveguide geometries is not, however, a new concept [52–69]. For example, in 1994, LC waveguides were fabricated using scanning force microscopy wherein the polymer alignment layers were intentionally "scratched" to introduce a refractive index profile in the LC layer that was suitable for an optical waveguide [53]. Silicon-on-insulator (SOI) configurations, such as those involving a high-index silicon waveguide on a low-index silicon oxide slab, can exhibit a single mode for operation at the Telecoms wavelength of 1,550 nm with minimal signal attenuation [62]. Due to the poor electro-optical effects in silicon, realizing tunable Si-based waveguides is very difficult. However, by combining SOI technology with LCs as the cladding material, it is possible to make devices tunable over a relatively large range with a small voltage [63,64]. Additionally, tunable waveguides realized by utilizing LCs as the core material have also been explored. For example, in the experiments of d'Alessandro, an integrated optical switch was demonstrated by fabricating V-shaped groove channels in silicon covered with an oxide and filled with an LC that can be switched with an applied voltage [65–67]. Subsequently, in 2015, methodologies for creating photonic channels on both silicon and polydimethylsiloxane (PDMS) were showcased, catering to the requirements of flexible devices. The propagation of polarization-independent light within a waveguide, with its core infused with LC, has also been reported [68,69]. A recent report has demonstrated various graded-index waveguides by controlling the spatial orientation of the director of nematic LCs. In this study, patterning of the LC using photoalignment (SD1) was employed to create straight and curved waveguides, as well as ring resonators [27].

Using LC materials provides the prospect of developing waveguides that consist of the same material for both the core and cladding, potentially offering greater flexibility and ease of integration into more complex architectures and device platforms. In this work, we have therefore developed LC waveguides by combining 2-photon direct laser writing (TPP-DLW) [70–73] and ultraviolet (UV) polymerization. To fabricate the waveguides, a voltage is applied to an LC layer to manipulate the director orientation before it is locked in place using laser writing. Upon removal of the voltage, the director orientation in the region surrounding the laser-written core relaxes back to a planar aligned configuration, resulting in a refractive index mismatch between the core and the cladding for incident light of a certain polarization. In this work, we first demonstrate a switchable LC waveguide, which can be made to appear or disappear with the application of a voltage. The transmission performance of the waveguide is then characterized to demonstrate that the transmission loss is relatively low over distances relevant to on-chip platforms. Such a switchable waveguide could be used as the basis for optical logic gates in optical computations. Following UV polymerization of the bulk LC layer, a conformable free-standing waveguide is presented, which is flexible and could be integrated into wearable technologies [40,43,74–80]. The stretchability of the material has been demonstrated in our previous work [80], so the waveguide device would also be stretchable.

Materials and Methods

To construct the waveguides, a custom-made glass cell was fabricated using 2 indium tin oxide (ITO)-coated substrates and a range of different spacer thicknesses, depending upon the requirements. The sample production process involved 3 main steps. First, a 1 wt % solution of polyvinyl alcohol (PVA) was spin-coated at a speed of approximately 1,900 revolutions per minute for 35 s onto 2 ITO-coated glass substrates, resulting in the formation of a thin polymer film on each substrate. Second, the substrates with the PVA layers were subjected to mechanical rubbing to induce a planar alignment layer. Afterward, the substrates with the ITO coating on the inner surfaces were sandwiched together separated by 2 spacers, the thickness of which is specified in the relevant sections. Finally, the sample was then sealed using UV-curable glue and wires were attached to the ITO electrodes to facilitate the application of an applied voltage. In this study, LC cells fabricated in-house were assembled so that the alignment layers on the inner surfaces of the top and bottom glass substrates were aligned so that the rubbing directions were anti-parallel. The resulting cell gap was then determined through the measurement of interference fringes recorded on a UV-Vis spectrometer (Agilent 8454).

The LC mixture employed in this study consisted of 3 main components: 69 wt % of the nematic LC mixture E7 (Synthon Chemicals Ltd.), 30 wt % of the reactive mesogen RM257 (1,4-bis-[4-(3-acryloyloxypropyloxy) benzoyloxy]-2-methylbenzene) (Synthon Chemicals Ltd.), and 1 wt % of the photoinitiator Irgacure 819 (Ciba-Geigy). These mixtures and compounds were first combined in an empty vial before being subjected to thermal diffusion by placing the resulting mixture in an oven at 70 to 75 °C for a period of around 12 h. On inspection, it was found that this process resulted in sufficient mixing of the constituents before the mixture was then capillary filled into the glass cells described above. The samples were further inspected on a polarizing optical microscope (POM) and subjected to a voltage to check that the mixtures had not been partially polymerized during the thermal diffusion process. The filled glass cells were then subsequently loaded into the TPP-DLW fabrication system for the inscription of the waveguides.

For the TPP-DLW in LCs, we have employed a custom-built system as depicted in Fig. S1. In short, the laser source was a titanium–sapphire femtosecond laser (Spectra-Physics Mai Tai) emitting at a wavelength (λ) of 780 nm. Mode locking resulted in pulses that had a duration of less than 100 fs with a repetition rate of 80 MHz. To minimize refractive index mismatches during fabrication, we carefully adjusted the linear polarization state of the laser to be perpendicular to the LC optic axis [80]. To write the waveguides into the LC layers, a relatively high optical power was focused into the bulk of the LC using an objective lens with numerical aperture (NA) of 0.45. This enabled 2-photon absorption to occur within a confined volume that was estimated to be 1 μm in the lateral dimension and 7 μm in the axial direction, which in turn triggered the cross-linking of the reactive mesogens through a free-radical polymerization reaction. Regions where the polymer network was formed then resulted in the LC alignment [74,80,81] becoming fixed. The waveguide core was then written by translating a 3-axis piezo Aerotech translation stage (ANT95XY-050 and ANT95V-3) relative to the focal region of the femtosecond laser with a positioning resolution of 1 nm and movement accuracy of 100 nm.

Waveguide fabrication

The fabrication process for the LC waveguides is depicted in Fig. 1A, where (i) to (iv) outline the steps for creating an electrically switchable LC waveguide, while steps (v) to (viii) illustrate the subsequent procedures for transforming the sample into a flexible waveguide. Following the capillary filling of the LC mixture [Fig. 1A(ii)], the glass cell was carefully positioned on a hotplate and heated to 70 °C for several minutes to ensure uniform filling of the LC mixture within the cell. The next step was to write a straight channel/waveguide with a nearly square shape cross-section such that the polymer network tethered to both glass substrates locking in a homeotropic alignment of the nematic LC in this region [as illustrated in Fig. 1A(iii)]. By applying a voltage during the fabrication process, the LC director rotates out of the plane of the substrates to form a homeotropic alignment. Writing the structure in the presence of a large applied voltage ensured that the homeotropic alignment of the nematic LC was preserved during laser exposure. By moving the LC sample at a speed of 100 μm/s during the fabrication process, a solid straight channel was created line-by-line and layer-by-layer under the influence of a relatively high voltage (50 V) [Fig. 1A(iii)]. This ensured the attainment of a homeotropic alignment in the nematic LC.

The core regions of the waveguide exhibited a higher refractive index, which is identical to the LC extraordinary refractive index ($n_e \approx 1.71$) when subjected to vertically polarized light relative to the plane of the substrates. These core regions were defined by the polymer-stabilized homeotropic nematic LC alignment, which had been locked-in through the laser writing process in the presence of an applied voltage, as shown in the inset of Fig. 1A(iii). On the other hand, the cladding region, characterized by a lower refractive index referring to the LC ordinary refractive index ($n_o \approx 1.54$) at 650 nm, consisted of a planar-aligned nematic LC in the absence of an applied voltage. By adjusting the applied voltage between 0 V and the fabrication voltage (50 V), the LC waveguide could be activated or deactivated accordingly [Fig. 1A(iv)]. Subsequently, the sample with the switchable LC waveguide underwent testing and characterization using a dedicated fiber coupling system, which will be further described in the following section.

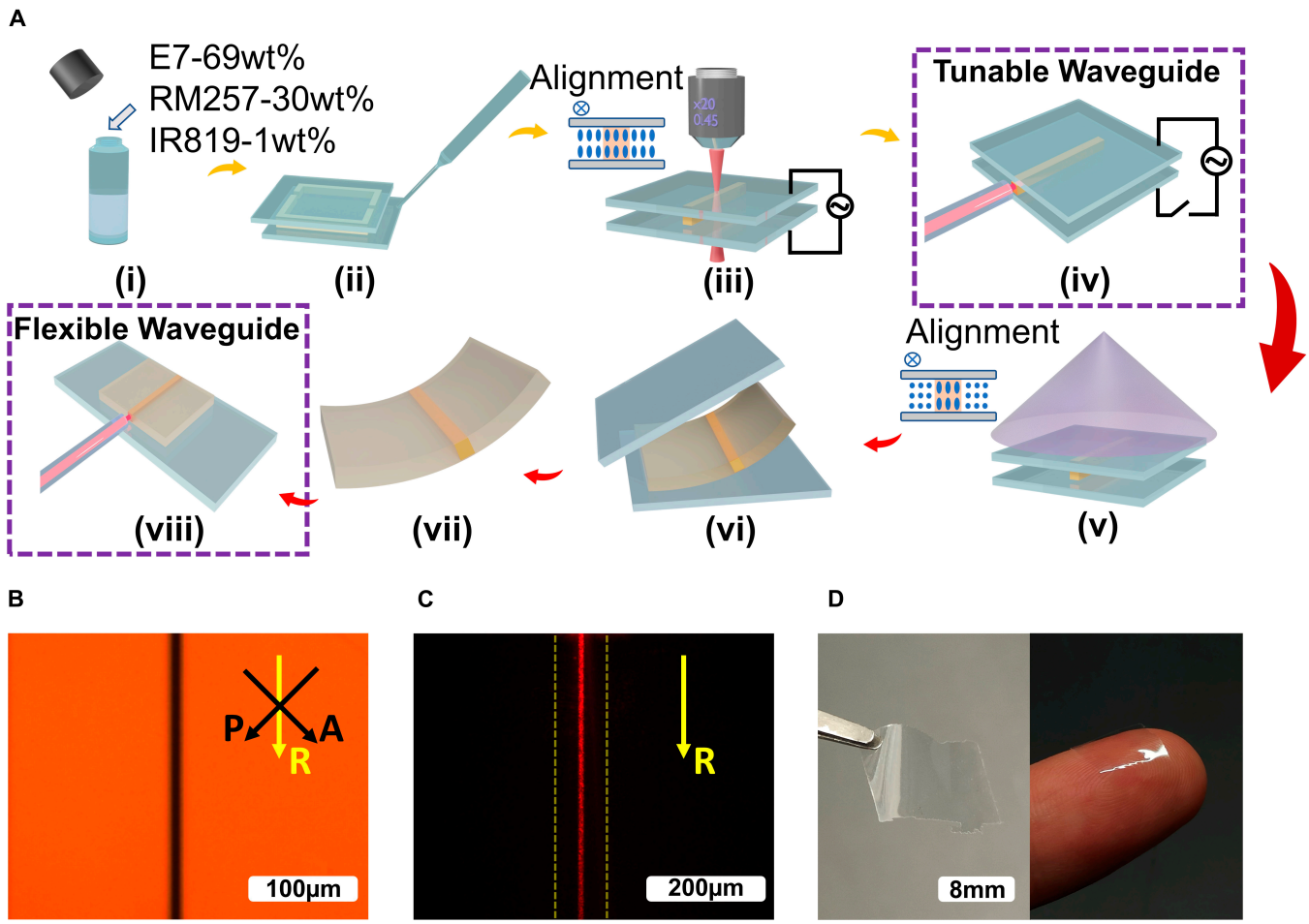

Fig. 1. Laser-written liquid crystal (LC) waveguide for voltage switching and mechanical flexibility. (A) Illustration of the fabrication process used to construct the voltage-switchable and deformable LC waveguides. The steps include (i) mixture preparation, (ii) capillary filling of LC mixture into glass cell, (iii) fabrication of an LC waveguide with a voltage applied to the LC cell, (iv) completion of the voltage-switchable waveguide, (v) bulk photo-polymerization of the film using UV illumination, (vi) delamination of the cell to form a free-standing LC film containing the waveguide, (vii) extraction of the flexible film, and (viii) completion of flexible LC waveguide for characterization. (B) POM images of the laser-written LC waveguide. The single-headed black arrows represent the orientations of the polarizer (P) and analyzer (A), whereas the single-headed yellow arrow represents the rubbing direction (R). (C) Photograph of the successful coupling of the output from the optical fiber into the LC waveguide when the ambient illumination is switched off. The dashed yellow lines indicate the region where the waveguide was written. (D) Photographs of a free-standing film with the laser-written waveguide after delamination.

Figure 1B presents a representative POM image of the optical texture when the LC waveguide sample was positioned between a pair of crossed polarizers, with the rubbing direction set at 45° to the transmission axes of the polarizers. The image was taken using a narrow bandpass filter with a central wavelength of 650 nm after the illumination source, which avoided any undesirable post-fabrication polymerization. In this case, no voltage was applied during the inspection. The image reveals a 10-μm-wide channel within a 14-μm-thick LC layer. The dark regions of the written channel indicate homeotropic alignment, while the adjacent bright regions indicate a planar alignment of the LC director. This observation is in accord with the predicted LC director profile obtained from simulations, which is described further shortly. Figure 1C presents a photograph of successful coupling when the ambient illumination was switched off and demonstration of the light propagation within the switchable laser-written waveguide.

The second configuration involved the demonstration and characterization of a flexible LC waveguide, with the fabrication process illustrated in Fig. 1A(v) to (viii). Following the formation of the homeotropic-aligned nematic LC channel, UV light was then illuminated on the sample to induce polymerization in the remaining unreacted regions (i.e., the cladding) of the sample [Fig. 1A(v)] when no voltage was applied. Specifically, the samples were photopolymerized using UV light with a peak wavelength of $\lambda = 365$ nm and a power density of 10 mW/cm^2 for 10 min. Therefore, the LC in the cladding region was polymerized in a planar-aligned state. Once the film was fully cross-linked, a scalpel was used to detach one corner of the sample [Fig. 1A(vi)]. The top glass substrate was removed, and the free-standing film was carefully extracted from the bottom glass layer using a razor blade and tweezers. A schematic of such a free-standing film with an embedded waveguide is presented in Fig. 1A(vii). Figure 1D presents a photograph captured by a digital single-lens reflex (SLR) camera, showcasing the flexible LC waveguide attached to a finger. For observation under a POM and coupling tests, the film was then adhered to a glass slide as shown in Fig. 1A(viii) from which it can then subsequently be peeled to investigate bent waveguide behavior.

Simulations based on the continuum theory and Euler–Lagrange approach were conducted to determine the tilt angle distribution of the LC director for both the laser-written regions, which consist of frozen-in homeotropic alignment due to the application of a high voltage (50 V) during fabrication and the nonpolymerized switchable regions surrounding the waveguide core. The simulations assumed a sample thickness of 14 μm and an initial pre-tilt angle of 4°. The one-constant approximation was applied for the elastic constants, with $K_{11} = K_{22} = K_{33} = K = 11.6$ pN. The director distribution as a function of the position within the plane of the waveguide cross-section and the surrounding regions of the sample will be illustrated in detail in the "Demonstration of waveguide activation and deactivation" section. For this geometrical configuration, incident light polarized perpendicular to the substrate surfaces experiences a higher extraordinary refractive index ($n_e = 1.71$) in the core regions and a lower ordinary refractive index ($n_o = 1.54$) at 650 nm in the switchable cladding regions. As the birefringence of E7 (Δn) is greater than zero, only the component of the incident light polarized parallel to the LC extraordinary axis satisfies the condition for total internal reflection (TIR) and can be confined within the channels, confirming the functionality of the channel as a light pipe/waveguide.

Waveguide characterization

To observe and characterize our switchable and flexible waveguide samples, we constructed a polarization-controlled fiber coupling system as depicted in Fig. 2A. A continuous-wave laser (180XL Visual Fault Locator Kit) emitting at 650 nm, originating from an optical fiber (core diameter = 9 μm), passed through a polarization controller to provide vertically linear polarized light perpendicular to the plane of the substrates. Two 3-axis stages from Thorlabs (MBT616D/M) were employed to facilitate the coupling of the beam from the output of the fiber directly into the laser-written waveguides. In order to image the sample, illumination from a quartz tungsten-halogen lamp (Thorlabs QTH10/M) was filtered using a long-pass filter to prevent any undesired polymerization during inspection. A complementary metal-oxide semiconductor (CMOS) camera (Thorlabs CS165CU/M) combined with an objective lens (NA = 0.12) in the microscope system was then utilized for image capture.

The microscope system positioned above the sample was designed for alignment of precise coupling of the output of the fiber with the laser-written waveguide at the edge of the sample when the illumination from the halogen lamp was on (Fig. 2B). It also enabled the intensity distribution along the written channel (14 μm × 10 μm × 3,000 μm) to be captured when the illumination from the lamp was turned off (Fig. 2C). As illustrated in Fig. 2C, when the 650-nm laser was coupled into the LC waveguide with incident light polarized perpendicular to the planar alignment surface, it effectively confined the light, preventing the beam from spreading out into the surrounding regions of the nonpolymerized LC. A comparison of incident light polarized parallel to the LC director in the core of the waveguide with the case when the incident polarization is misaligned with the LC director is presented in Fig. S2.

Results and Discussion

Demonstration of a laser-written waveguide

To assess the performance of the LC waveguides, we considered a 10-μm-wide waveguide fabricated within a 14-μm-thick cell. Figure 3A presents a representative POM image of the laser-written waveguide in the upper panel, accompanied by the corresponding image depicting propagation of $\lambda = 650$-nm light in the lower image panel. The laser writing power used to fabricate the waveguide was set at 49 mW. In the study, the propagation attenuation along the waveguide was determined by the intensity of scattered light rather than a direct measurement of the power within the waveguide. Generally, the light intensity declines exponentially along the propagation distance. By extracting the intensity profile along the selected waveguide, the loss factor (expressed in dB) can be determined using the following formula:

$$\text{Loss} = 10\log_{10}{}^{B}\!/_{A} \quad (1)$$

where A and B represent the intensity at the starting point (as defined below) and intensity at the position on the waveguide being examined, respectively, when the energy flow propagated from position A to B with a constant attenuation. This was determined by weakly scattered light captured by the microscope system in Fig. 2A. In the study, the intensity loss near the coupling entrance was found to be relatively large due to the imperfect nature of the coupling between the optical fiber and the waveguide. As a result, regions of the waveguide located slightly away from the entrance were typically chosen for analysis to

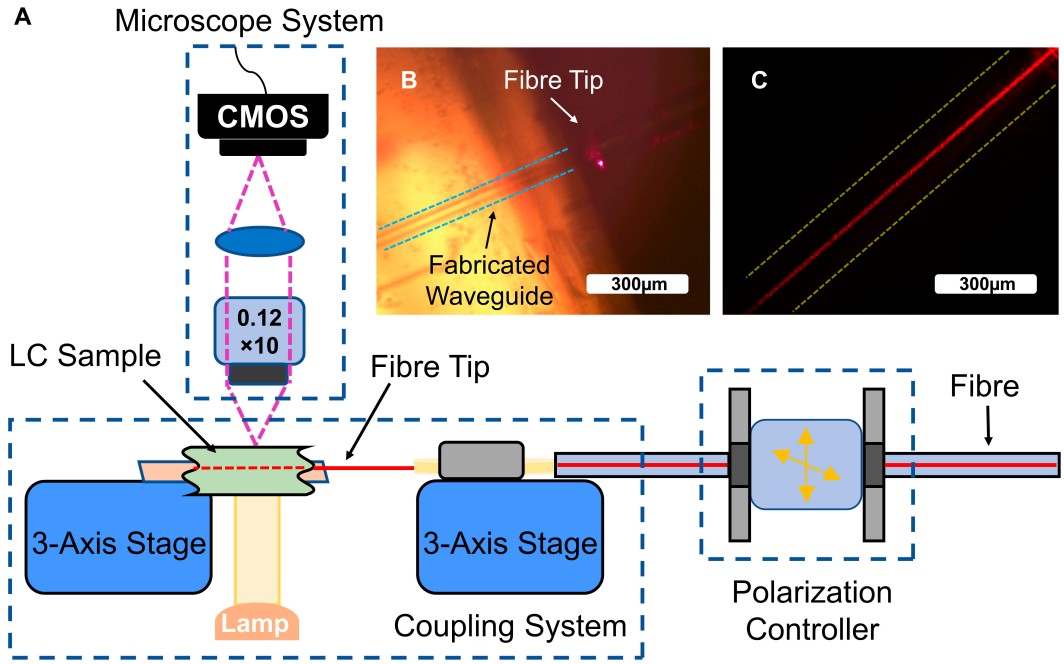

Fig. 2. Characterizing the laser-written LC waveguides. (A) Schematic of the experimental setup used to couple the laser emission ($\lambda = 650$ nm) from the optical fiber into the laser-written channel. The light in the optical fiber first travels through a polarization controller to generate a beam with a polarization such that it is aligned along the director in the laser-written waveguide. The beam from the optical fiber is then coupled into the fabricated structures with the aid of 2 three-axis translation stages. A microscope system was used for image capture and data analysis presented in this work. (B) Microscope image, which illustrates the positioning of the optical fiber relative to the LC waveguide. The dashed blue lines indicate the region where the waveguide was written. (C) Photograph of successful coupling of the output from the optical fiber into the LC waveguide. The dashed yellow lines represent the laser-written polymer regions.

determine the intensity loss. In Fig. 3A, the position labeled with "0 μm" refers to the starting point "*A*." The loss in dB at each examined position along the waveguide (referred to as "*B*") was defined by Eq. 1. Consequently, in this example, the intensity loss at $\lambda = 650$ nm was confirmed to be −1.8 dB/mm (Fig. 3B). The intensity variation with distance along the waveguide, shown in blue, was fitted with a linear function depicted by the red line in Fig. 3B.

Varying the waveguide fabrication parameters

In addition to the demonstration and characterization of a single straight waveguide in the LC layer, the performances for different fabrication configurations, such as channel geometry sizes and different laser writing powers, were also investigated. Figure 4A investigates 4 different waveguides with varying core widths ranging from 10 to 40 μm. All waveguides were fabricated along a direction parallel to the LC rubbing direction to ensure a refractive index difference between the fabricated (core) and the surrounding regions (cladding) when illuminated by light that was polarized perpendicular to the substrates. The results indicate that waveguide channels with narrower core widths exhibit less intensity attenuation and improved power confinement.

Other features were also observed. First, at the front of the waveguide (≈0.2 mm), the difference in width is minimal and there is then an inconsistency in the slope. This is associated with an "edge" effect in our waveguides due to the difficulty of writing the waveguides close to the edge of the LC cell using the TPP-DLW process. This could explain the reason for why all of the waveguides behave the same at the front of the cell. The kink in the plots in Fig. 4 represent the point where the light starts to be guided in the "well-written" regions away from the edge of the device. Second, there is a nonlinearity in the loss as a function of distance, especially for the narrowest waveguide. We associate this with some inconsistency in the waveguide structure along the length of the core, which leads to some variance in loss. Therefore, due to these 2 features, for the results presented (Figs. 3 and 4B and C), we always checked the waveguides for consistent behavior along the length and focused on the regions slightly away from the entrance of the LC cell for further analysis.

Figure 4B illustrates the intensity attenuation along straight waveguides for a core of 20 μm width fabricated at different writing powers (42, 49, 56, and 63 mW) in a thicker LC layer (24 μm). Similarly, Fig. 4C compares the performance of 10-μm-wide waveguides in a thinner LC layer (i.e.,14 μm thick). The reason for narrowing the geometric size in 2 dimensions was to maintain the relative size of the cross-section.

The results show that the laser-written LC waveguides function consistently and exhibit minimal differences in loss attenuation for waveguides fabricated with writing powers ranging from 42 to 63 mW. In practice, a relatively low writing power (less than 42 mW) results in weak polymerization that results in insufficient tethering to the glass substrates. Conversely, a writing power that was too high (more than 63 mW) leads to apparent irreversible damage to the LC device whereby isotropic bubbles form along the trajectory of the laser writing, which does not change in the presence of an electric field. This observation holds true for both the thinner (14 μm) and thicker (24 μm) LC layers. It can be noted that the smaller geometry cross-section size leads to less intensity loss. When compared with the waveguides with a larger cross-section in Fig. 4B, the waveguide with a smaller geometric size in Fig. 4C exhibits a better performance in terms of intensity attenuation. It is notable in Fig. 4B and C

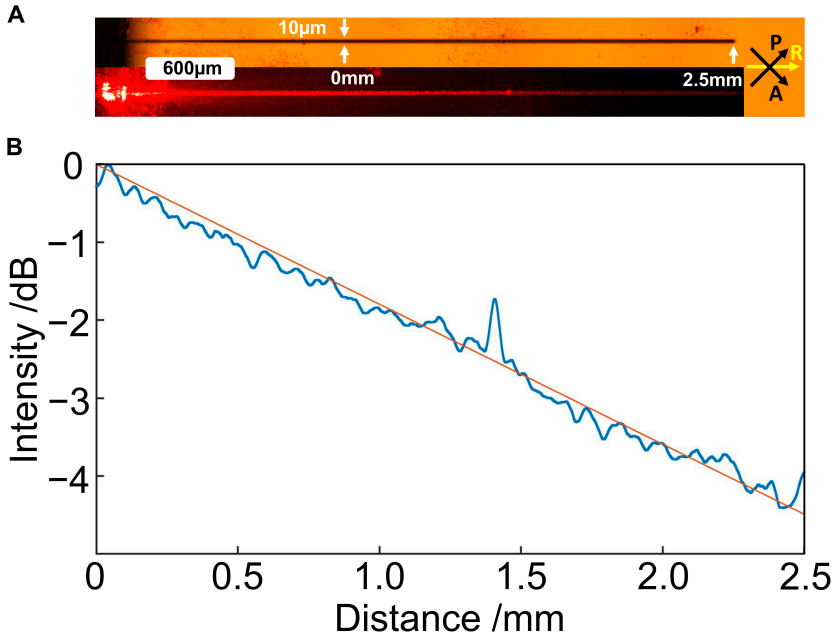

Fig. 3. Waveguiding of light in a laser-written LC waveguide. (A) POM image of the laser-written waveguide fabricated with a power of 49 mW (upper image) and corresponding image of light propagation of $\lambda = 650$-nm laser light in the waveguide (lower image). (B) Plot of the intensity loss (in dB) along the waveguide extracted from the lower image in (A).

that the intensity reduces by around 44% after propagation of 1,000 μm in the sample of a larger cross-section (Fig. 4B), while that in the sample with a smaller cross-section (Fig. 4C) only attenuates by around 37% at an identical distance, which agrees with the result in Fig. 4A.

Demonstration of waveguide activation and deactivation

One of the key novelties of this work is the electric switchability of the laser-written waveguides, which is demonstrated and confirmed. The waveguide investigated here had a width of 10 μm and was fabricated in a 14-μm-thick LC layer with an applied voltage of 50 V during fabrication. Figure 5A shows the switching property comparison and presents the propagation image, POM image with crossed polarizers, and LC director simulation results when no voltage was applied. These results allow for the verification of the designed LC director distribution and confirm the power confinement within the waveguide. In contrast, Fig. 5B shows the corresponding results when a voltage was applied, indicating that the LC director in the LC layer aligned homeotropically throughout the bulk, and the incident light no longer encounters a refractive index difference. As a result, the light along the laser-written structure rapidly spreads out as it is no longer able to guide the wave. Figure 5C compares the confinement capability of the laser-written waveguide between 2 states, which refer to voltage on and off. The subplots embedded in the images indicate the intensity distributions across the waveguide at the positions labeled with yellow dashed lines. Notably, with an applied voltage on, the waveguide loses the capacity for optical confinement along the structures compared with a similar situation when the voltage is switched off. It was found that the ratio of the intensity in a small region at the end of the waveguide to that close to the entrance drastically drops to a low value when the applied voltage was gradually increased. From Fig. 5D, a minimum transition voltage of 2.5 V at which the waveguide starts to lose the ability to confine energy can be confirmed. Since the Fréedericksz threshold voltage of the sample typically falls within the range of 0.7 to 1 V, it is evident that the conversion voltage is significantly higher than the threshold voltage, which means that, at the beginning of the switching, the LCs cannot be tilted sufficiently to generate a refractive index mismatch. Therefore, the waveguide would not lose the ability to confine the light for relatively low applied voltage amplitudes.

Demonstration of a flexible waveguide

The demonstration and characterization of an in-film flexible waveguide is another key aspect that we aim to illustrate in this work. After creating a localized polymer structure with the laser to lock in the homeotropically aligned waveguide region at a high voltage, the remaining LC polymer mixture was then polymerized with UV light without voltage to ensure TIR, as described in the "Waveguide fabrication" section. According to the conclusions presented in the "Varying the waveguide fabrication parameters" section, a waveguide with a smaller cross-sectional size exhibits less intensity attenuation. However, challenges related to the detachment, extraction, and transfer of the film during experiments restricted the actual minimum achievable film thickness in this study. Here, we demonstrate and characterize a 20-μm-wide waveguide in a 20-μm-thick free-standing film. We utilized a scalpel to trim the end face of the LC film to make it as smooth as possible (akin to polishing the end face of a waveguide written into hard materials). Subsequently, the flexible waveguide was coupled to the fiber tip, which had been polished using a fiber optic cleaver. Figure 6A is a photograph showing light propagation within a laser-written channel in a curved flexible film, with the inset POM image located at the top-right corner from which it is notable that the LC is aligned differently within the fabricated and nonlaser fabricated regions. Figure 6B presents the laser-written waveguide coupled with vertically polarized incident light relative to the

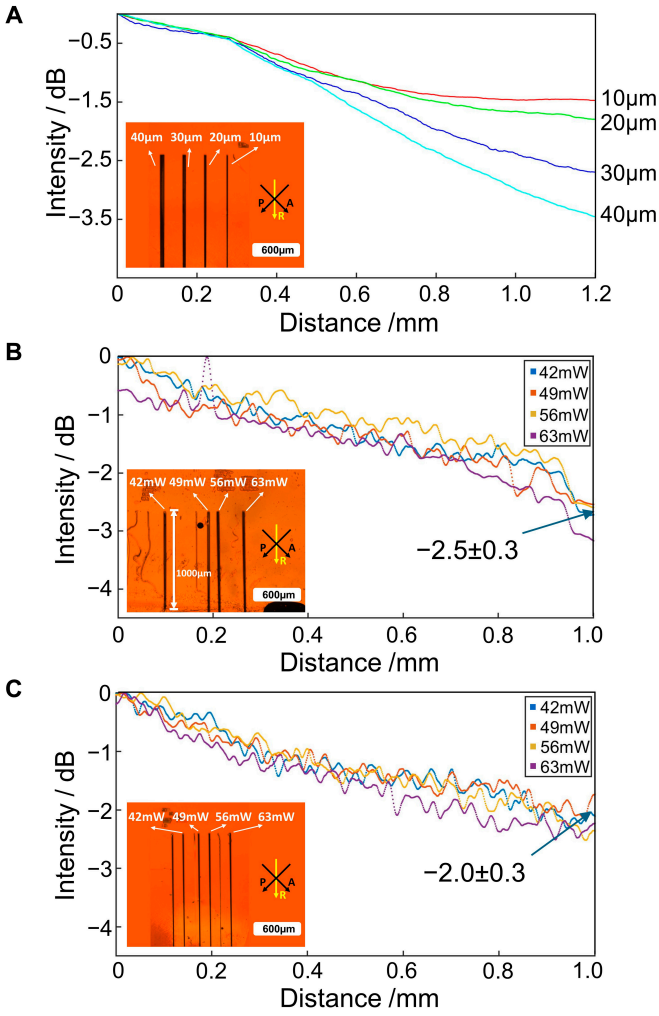

Fig. 4. Varying the laser-written LC waveguide parameters. (A) Plot of the intensity attenuation along the waveguide for waveguides of different widths ranging from 10 to 40 μm written at 49 mW in a 14-μm-thick LC layer. (B and C) Intensity attenuation as a function of the distance along the waveguide for those fabricated at different writing powers (42, 49, 56, and 63 mW) in 24- and 14-μm-thick LC layers, respectively. Insets show POM images of these different waveguides.

substrates, both with and without illumination from the halogen lamp. The yellow dashed lines indicate the spatial extent of the channel. Figure S3 provides images of the free-standing LC waveguide misaligned with the fiber tip for comparison.

Figure 6C showcases photographs captured by the SLR camera of a 5-mm-long flexible waveguide for both flat and bent film configurations. For the flat film configuration, it is evident that the intensity is confined within the waveguide and propagates along its path. In contrast, to demonstrate flexibility, curvature was applied to deform the film. Subsequently, the lower image in Fig. 6C not only confirms the functionality of the waveguide when the film is bent but also demonstrates its flexibility. Figure S4 presents results for the case when the incident light is not correctly coupled into the waveguides for both flat and bent film geometries, showing a divergence of the light, further highlighting the functionality and flexibility of the waveguide.

Figure 6D provides the intensity loss in dB as a function of distance along the flexible waveguide. In this case, the loss factor is approximately −0.2 dB/mm for $\lambda = 650$ nm. Compared with the intensity attenuation in the LC sample in Fig. 3A, the loss factor is significantly reduced. The underlying reason was hypothesized to be the change of the top and bottom claddings from glass to air, resulting in a reduced cladding refractive index and consequently leading to diminished losses after the delamination process. Figure 6D compares the confinement capability when the written waveguide was successfully coupled and when it was deliberately misaligned. The embedded plot represents the intensity profile of the cross-section labeled with the yellow dashed lines. Compared with the misaligned situation, it is notable that the coupled waveguide can confine the light even after a relatively long propagation distance. The results confirm the functionality of the waveguide with proof, further validating its performance.

Conclusion

In conclusion, we have proposed fabrication strategies for an electrically switchable LC waveguide and a free-standing flexible LC waveguide, utilizing a combination of TPP-DLW and UV bulk polymerization technologies. Unlike most existing tunable LC waveguide geometries, our waveguides are based solely on LC materials, which means both the cladding and core are made from the same LC mixture. We have successfully demonstrated the electrical switchability and mechanical flexibility of the laser-written LC waveguides with satisfactory performance. Additionally, we have investigated the intensity attenuation of the waveguide for different parameters, such as LC layer thickness, laser writing power, and channel width of the waveguide core.

The switchability of the on-chip waveguide has potential applications in optical computing and beam steering, while the flexible waveguide shows promise for on-skin sensors and brain–computer interfaces [53,58,82–86]. Our findings indicate that a smaller channel geometry size leads to better intensity attenuation, and we determined that a 10-μm straight channel in a 14-μm-thick LC layer has a loss factor of −1.8 dB/mm for $\lambda = 650$ nm. For the flexible LC waveguide, we verified an intensity loss of −0.2 dB/mm for a straight waveguide with a cross-section of 20 μm × 20 μm. These results highlight the considerable potential of electrically sensitive and mechano-optical on-chip LC devices fabricated using laser writing and UV-assisted polymer network formation. In subsequent investigations, it would be desirable to consider waveguides exhibiting diverse geometric configurations, including bent waveguides, multi-layered waveguides, and beam splitters fabricated using the TPP-DLW process. Additionally, further exploration of the stability of the obtained waveguides under varying conditions such as temperature and humidity would also be beneficial for future applications. Increasing the fabrication speed and implementing parallelization would significantly accelerate the fabrication process and enable the fabrication of longer waveguides in the future. For the stretchable films, we expect that stretching would lead to a decrease in the cross-sectional size of the waveguide, resulting in a shorter cutoff wavelength. Additionally, positive strain usually leads to an increase in the refractive index not only in the core but also in the cladding region. However, the influence of stretching on birefringence and cutoff frequency requires further investigation. Lastly, the approach presented in this paper could lead to further advancement of LC-based waveguides and showcase their potential for next-generation photonic applications.

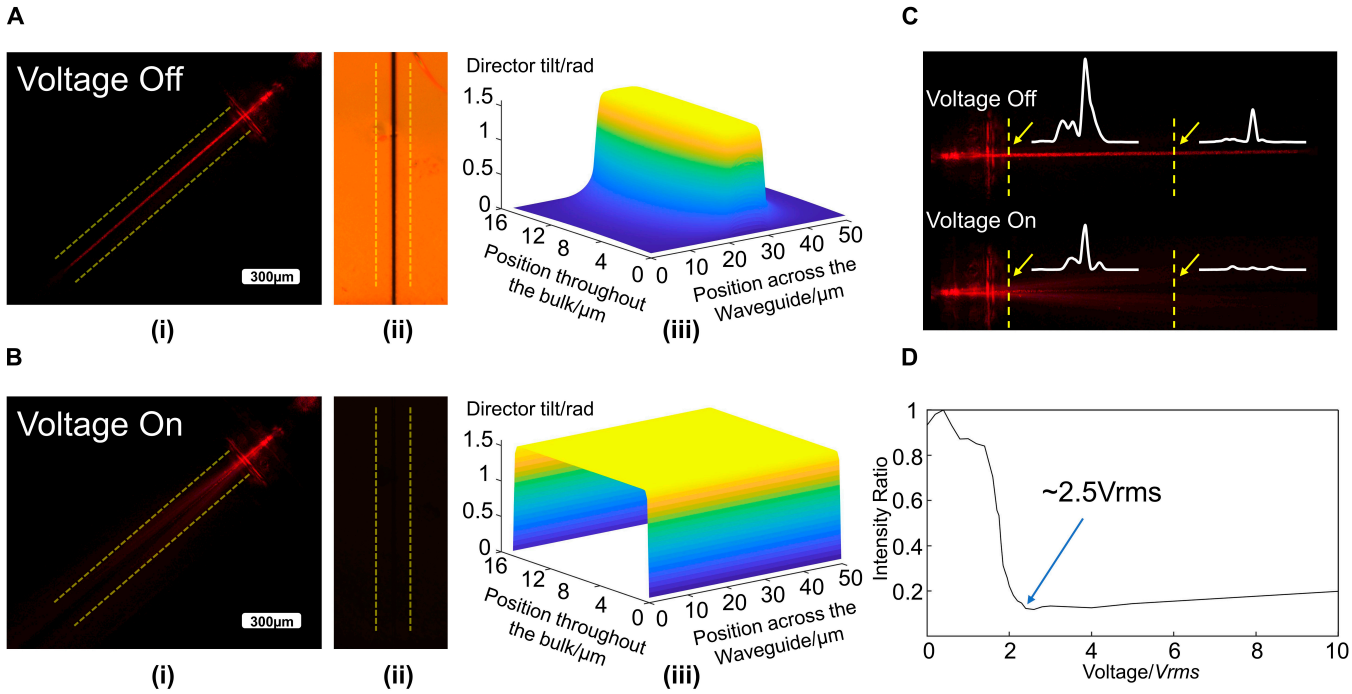

Fig. 5. Voltage switching of a laser-written LC waveguide. (A) Photograph and POM image of the LC waveguide for no applied voltage and (B) the case when waveguiding vanishes when a voltage is applied to the LC device. (i) Microscope images of coupling for the voltage off and on states. (ii) POM images of the voltage on and off states. (iii) Simulation results of the LC director distribution within and around the waveguide for the voltage off and on states. (C) This panel compares the intensity profiles of the cross-section labeled with yellow dashed lines between the situations of voltage on and off. (D) Normalized intensity ratio of the region at the end of the channel to that close to the edge when the applied voltage is gradually increased.

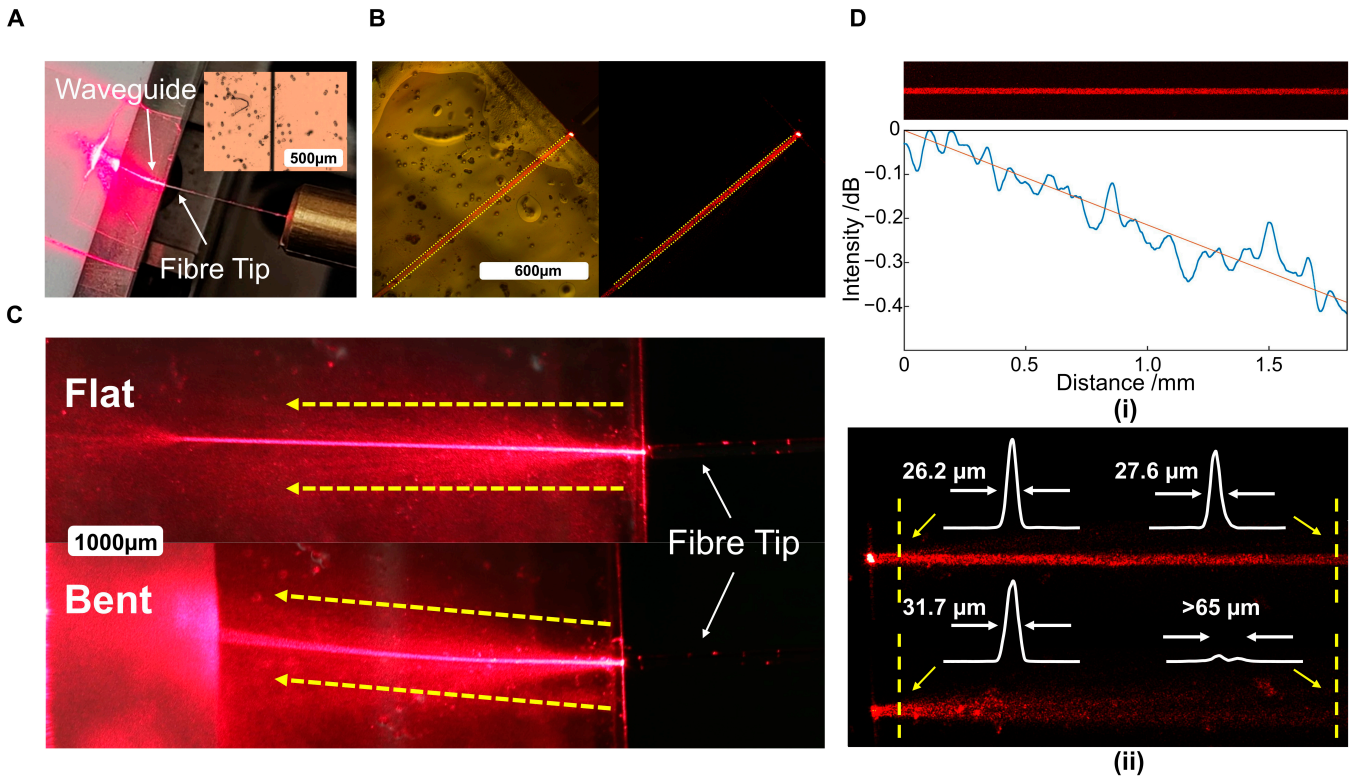

Fig. 6. Demonstration and characterization of a flexible laser-written LC waveguide. (A) Photograph demonstrating that the coupled light propagates within a written channel on a curved film. The POM image of the flexible waveguide is shown in the top-right corner. (B) The functionality of the waveguide is maintained in a free-standing film. (C) Photographs comparing the light propagation in waveguides for flat and bent configurations. (D) Characterization of a flexible LC waveguide: (i) intensity attenuation in dB as a function of propagation distance and (ii) intensity profiles in the cross-section labeled with yellow dashed lines between the coupled and misaligned situations within the flexible film. The full width at half maximum is represented by the white labels.

Acknowledgments

Funding: This research was funded in whole, or in part, by the UKRI (EP/R004803/01, P.S.S.; EP/R511742/1, S.M.M., S.J.E., and M.J.B.). For the purpose of Open Access, the author has applied a CC BY public copyright license to any Author Accepted Manuscript version arising from this submission. This research was also supported by the John Fell Fund (Oxford University Press) and The Royal Society (UK), which provided resources for the laser writing facility.
Author contributions: Conceptualization: B.C., P.X., S.J.E., and S.M.M. Methodology: B.C., P.X., S.J.E., and S.M.M. Validation: B.C., P.X., Z.Z., and S.J.E. Visualization: B.C. Formal analysis: B.C., P.X., Z.Z., and S.J.E. Investigation: B.C., P.X., Z.Z., S.J.E., and S.M.M. Resources: P.X., P.S.S., M.L., L.X., X.Q., M.J.B., S.J.E., and S.M.M. Data curation: B.C., P.X., and S.J.E. Writing—original draft preparation: B.C., P.X., and S.M.M. Writing—review and editing: B.C., P.X., S.J.E., and S.M.M. Supervision: P.X., S.J.E., and S.M.M. Project administration: P.X., S.J.E., and S.M.M. Funding acquisition: S.M.M., P.S.S., S.J.E., and M.J.B. All authors have read and agreed to the published version of the manuscript.
Competing interests: The authors declare that they have no competing interests.

Data Availability

All data are available upon request to the corresponding authors.

Supplementary Materials

Figs. S1 to S4

References

1. Xia Y, Whitesides GM. Soft lithography. *Annu Rev Mater Sci*. 1998;28:153–184.
2. Singh M, Haverinen HM, Dhagat P, Jabbour GE. Inkjet printing-process and its applications. *Adv Mater*. 2010;22(6):673–685.
3. del Pozo M, Sol JAHP, Schenning APHJ, Debije MG. 4D printing of liquid crystals: What's right for me? *Adv Mater.* 2022;34(3):e2104390.
4. Mkhize N, Bhaskaran H. Electrohydrodynamic jet printing: Introductory concepts and considerations. *Small Sci*. 2022;2(2):2100073.
5. Reizabal A, Tandon B, Lanceros-Méndez S, Dalton PD. Electrohydrodynamic 3D printing of aqueous solutions. *Small*. 2023;19(7):Article e2205255.
6. Jandyal A, Chaturvedi I, Wazir I, Raina A, Ul Haq MI. 3D printing—A review of processes, materials and applications in industry 4.0. *Sustain Oper Comput*. 2022;3:33–42.
7. Saadi MASR, Maguire A, Pottackal NT, Thakur MSH, Ikram MM, Hart AJ, Ajayan PM, Rahman MM. Direct ink writing: A 3D printing technology for diverse materials. *Adv Mater*. 2022;34(28):Article e2108855.
8. Liu Z, Li M, Dong X, Ren Z, Hu W, Sitti M. Creating three-dimensional magnetic functional microdevices via molding-integrated direct laser writing. *Nat Commun*. 2022;13(1):2016.
9. Sedghamiz E, Liu M, Wenzel W. Challenges and limits of mechanical stability in 3D direct laser writing. *Nat Commun*. 2022;13(1):2115.
10. del Pozo M, Delaney C, Pilz da Cunha M, Debije MG, Florea L, Schenning APHJ. Temperature-responsive 4D liquid crystal microactuators fabricated by direct laser writing by two-photon polymerization. *Small Struct.* 2022;3(2):2100158.
11. Rao DGS, Palacharla V, Swarnakar S, Kumar S. Design of all-optical D flip-flop using photonic crystal waveguides for optical computing and networking. *Appl Optics*. 2020;59(23):7139–7143.
12. Wang X, Xie P, Chen B, Zhang X. Chip-based high-dimensional optical neural network. *Nano-Micro Lett.* 2022;14(1):221.
13. Liu Y, Wang P, Wang Y, Lin Z, Liu H, Huang J, Huang Y, Duan X. van der Waals integrated devices based on nanomembranes of 3D materials. *Nano Lett*. 2020;20(2):1410–1416.
14. Ni Y, Chen C, Wen S, Xue X, Sun L, Yang Y. Computational spectropolarimetry with a tunable liquid crystal metasurface. *eLight*. 2022;2:23.
15. Meng Y, Chen Y, Lu L, Ding Y, Cusano A, Fan JA, Hu Q, Wang K, Xie Z, Liu Z, et al. Optical meta-waveguides for integrated photonics and beyond. *Light Sci Appl*. 2021;10(1):235.
16. Huang Y, Xu Y, Bisoyi HK, Liu Z, Wang J, Tao Y, Yang T, Huang S, Yang H, Li Q. Photocontrollable elongation actuation of liquid crystal elastomer films with well-defined crease structures. *Adv Mater.* 2023;35(36):Article e2304378.
17. Ma L-L, Li CY, Pan JT, Ji YE, Jiang C, Zheng R, Wang ZY, Wang Y, Li BX, Lu YQ. Self-assembled liquid crystal architectures for soft matter photonics. *Light Sci Appl.* 2022;11(1):270.
18. Chen J, Xiong Y, Xu F, Lu Y. Silica optical fiber integrated with two-dimensional materials: Towards opto-electro-mechanical technology. *Light Sci Appl*. 2021;10(1):78.
19. Zhou S, Shen Z, Li X, Ge S, Lu Y, Hu W. Liquid crystal integrated metalens with dynamic focusing property. *Opt Lett*. 2020;45(15):4324–4327.
20. Zhu S, Chen X, Liu X, Zhang G, Tian P. Recent progress in and perspectives of underwater wireless optical communication. *Prog Quantum Electron.* 2020;73:Article 100274.
21. He J, Dong T, Xu Y. Review of photonic integrated optical phased arrays for space optical communication. *IEEE Access*. 2020;8:188284–188298.
22. Zhu Z, Janasik M, Fyffe A, Hay D, Zhou Y, Kantor B, Winder T, Boyd RW, Leuchs G, Shi Z. Compensation-free high-dimensional free-space optical communication using turbulence-resilient vector beams. *Nat Commun*. 2021;12(1):1666.
23. Yu B-Y, Yue DW, Hou KX, Ju L, Chen H, Ding C, Liu ZG, Dai YQ, Bisoyi HK, Guan YS, et al. Stretchable and self-healable spoof plasmonic meta-waveguide for wearable wireless communication system. *Light Sci Appl*. 2022;11(1):307.
24. Zola RS, Bisoyi HK, Wang H, Urbas AM, Bunning TJ, Li Q. Dynamic control of light direction enabled by stimuli-responsive liquid crystal gratings. *Adv Mater*. 2019;31:Article e1806172.
25. Xiong J, Wu S-T. Planar liquid crystal polarization optics for augmented reality and virtual reality: From fundamentals to applications. *eLight*. 2021;1:3.
26. Jisha CP, Arumugam SV, Marrucci L, Nolte S, Alberucci A. Waveguiding driven by the Pancharatnam-Berry phase. *Phys Rev A*. 2023;107:Article 013523.
27. Wei T, Chen P, Tang MJ, Wu GX, Chen ZX, Shen ZX, Ge SJ, Xu F, Hu W, Lu YQ. Liquid-crystal-mediated active waveguides

toward programmable integrated optics. *Adv Opt Mater*. 2020;8(10):1902033.
28. Chen S, Zhuo M-P, Wang X-D, Wei G-Q, Liao L-S. Optical waveguides based on one-dimensional organic crystals. *PhotoniX*. 2021;2:2.
29. Annadhasan M, Basak S, Chandrasekhar N, Chandrasekar R. Next-generation organic photonics: The emergence of flexible crystal optical waveguides. *Adv Opt Mater*. 2020;8(21):2000959.
30. Tian D, Chen Y. Optical waveguides in organic crystals of polycyclic arenes. *Adv Opt Mater*. 2021;9(23):2002264.
31. Wu S, Zhou B, Yan D. Recent advances on molecular crystalline luminescent materials for optical waveguides. *Adv Opt Mater.* 2021;9(23):2001768.
32. Hsiang E-L, Wu S-T. Novel developments in computational spectropolarimeter. *Light Sci Appl*. 2023;12(1):52.
33. Jain P, Honnungar RV. A review on materials for integrated optical waveguides. Paper presented at: Proceedings of Fourth International Conference on Inventive Material Science Applications. Advances in Sustainability Science and Technology; 2021 Oct. 20; Springer Singapore.
34. Chakravarty S, Teng M, Safian R, Zhuang L. Hybrid material integration in silicon photonic integrated circuits. *J Semicond*. 2021;42:Article 041303.
35. Ding Y, Li Y, Yang Q, Wu S. Design optimization of polarization volume gratings for full-color waveguide-based augmented reality displays. *J Soc Inf Disp*. 2023;31(5):380–386.
36. Chen X, Li C, Tsang HK. Device engineering for silicon photonics. *NPG Asia Mater*. 2011;3:34–40.
37. Bogaerts W, Chrostowski L. Silicon photonics circuit design: Methods, tools and challenges. *Laser Photon Rev*. 2018;12(4):1700237.
38. Zheng R, Ma L, Feng W, Pan J, Wang Z, Chen Z, Zhang Y, Li C, Chen P, Bisoyi HK, et al. Autonomous self-sustained liquid crystal actuators enabling active photonic applications. *Adv Funct Mater*. 2023;33(38):2301142.
39. Bisoyi HK, Li Q. Liquid crystals: Versatile self-organized smart soft materials. *Chem. Rev.* 2022;122(5):4887–4926.
40. Yin K, Hsiang EL, Zou J, Li Y, Yang Z, Yang Q, Lai PC, Lin CL, Wu ST. Advanced liquid crystal devices for augmented reality and virtual reality displays: Principles and applications. *Light Sci Appl*. 2022;11(1):161.
41. Xiong J, Yang Q, Li Y, Wu S-T. Holo-imprinting polarization optics with a reflective liquid crystal hologram template. *Light Sci Appl*. 2022;11(1):54.
42. Zhang X, Xu Y, Valenzuela C, Zhang X, Wang L, Feng W, Li Q. Liquid crystal-templated chiral nanomaterials: From chiral plasmonics to circularly polarized luminescence. *Light Sci Appl*. 2022;11(1):223.
43. Coles H, Morris S. Liquid-crystal lasers. *Nat Photonics*. 2010;4:676–685.
44. Chen X-M, Feng WJ, Bisoyi HK, Zhang S, Chen X, Yang H, Li Q. Light-activated photodeformable supramolecular dissipative self-assemblies. *Nat Commun*. 2022;13:3216.
45. Wei B, Zhang Y, Li P, Liu S, Hu W, Lu Y, Wu Y, Dou X, Zhao J. Liquid-crystal splitter for generating and separating autofocusing and autodefocusing circular Airy beams. *Opt Express*. 2020;28(18):26151–26160.
46. Li S, Bai H, Liu Z, Zhang X, Huang C, Wiesner LW, Silberstein M, Shepherd RF. Digital light processing of liquid crystal elastomers for self-sensing artificial muscles. *Sci Adv*. 2021;7(30):Article eabg3677.
47. Wu J, Wu SB, Cao HM, Chen QM, Lu YQ, Hu W. Electrically tunable microlens array enabled by polymer-stabilized smectic hierarchical architectures. *Adv Opt Mater*. 2022;10(20): 2201015.
48. Bolis S, Gorza SP, Elston SJ, Neyts K, Kockaert P, Beeckman J. Spatial fluctuations of optical solitons due to long-range correlated dielectric perturbations in liquid crystals. *Phys Rev A*. 2017;96:Article 031803.
49. Du F, Lu Y-Q, Wu S-T. Electrically tunable liquid-crystal photonic crystal fiber. *Appl Phys Lett.* 2004;85:2181–2183.
50. Chen P, Wei B, Hu W, Lu Y. Liquid-crystal-mediated geometric phase: From transmissive to broadband reflective planar optics. *Adv Mater*. 2020;32(27):Article e1903665.
51. Zografopoulos DC, Asquini R, Kriezis EE, D'Alessandro A, Beccherelli R. Guided-wave liquid-crystal photonics. *Lab Chip*. 2012;12(19):3598.
52. Lammers K, Alberucci A, Pannian J, Szameit A, Nolte S. Hybridization of femtosecond-laser written waveguides with liquid crystals. Optica Open. Preprint. 2023.
53. Rüetschi M, Grütter P, Fünfschilling J, Güntherodt H-J. Creation of liquid crystal waveguides with scanning force microscopy. *Science*. 1994;265(5171):512–514.
54. Whinnery J, Chenming H, Kwon Y. Liquid-crystal waveguides for integrated optics. *IEEE J Quantum Electron*. 1977;13(4):262–267.
55. Hu C, Whinnery JR. Losses of a nematic liquid-crystal optical waveguide*. *J Opt Soc Am*. 1974;64(11):1424–1432.
56. Asquini R, Fratalocchi A, D'Alessandro A, Assanto G. Electro-optic routing in a nematic liquid-crystal waveguide. *Appl Optics*. 2005;44(19):4136–4143.
57. Park H-G, Barrelet CJ, Wu Y, Tian B, Qian F, Lieber CM. A wavelength-selective photonic-crystal waveguide coupled to a nanowire light source. *Nat Photonics*. 2008;2: 622–626.
58. Fratalocchi A, Assanto G, Brzdąkiewicz KA, Karpierz MA. Optical multiband vector breathers in tunable waveguide arrays. *Opt Lett*. 2005;30(2):174–176.
59. Kasano M, Ozaki M, Yoshino K, Ganzke D, Haase W. Electrically tunable waveguide laser based on ferroelectric liquid crystal. *Appl Phys Lett*. 2003;82:4026–4028.
60. Presnyakov VV, Liu ZJ, Chigrinov VG. Infiltration of photonic crystal fiber with liquid crystals. Paper presented at: Proc. SPIE 6017, Nanophotonics for Communication: Materials and Devices II, 60170J; 2005; Boston, MA, USA.
61. Beeckman J, James R, Fernandez FA, de Cort W, Vanbrabant PJM, Neyts K. Calculation of fully anisotropic liquid crystal waveguide modes. *J Light Technol*. 2009;27(17):3812–3819.
62. Beeckman J. Liquid-crystal photonic applications. *Opt Eng.* 2011;50(8):Article 081202.
63. Bogaerts W, Adamski A, Beeckman J, Neyts K, Baets R. Silicon-on-insulator optical waveguides with liquid crystal cladding for switching and tuning. Paper presented at: Proceedings of the European Conference on Optical Communications; 2003.
64. De Cort W, Beeckman J, James R, Fernández FA, Baets R, Neyts K. Tuning of silicon-on-insulator ring resonators with liquid crystal cladding using the longitudinal field component. *Opt Lett*. 2009;34(13):2054.
65. d'Alessandro A, Bellini B, Donisi D, Beccherelli R, Asquini R. Nematic liquid crystal optical channel waveguides on silicon. *IEEE J Quantum Electron*. 2006;42(10):1084–1090.

66. Donisi D, Bellini B, Beccherelli R, Asquini R, Gilardi G, Trotta M, d'Alessandro A. A switchable liquid-crystal optical channel waveguide on silicon. *IEEE J. Quantum Electron.* 2010;46(5):762–768.
67. Cai D-P, Nien S-C, Chiu H-K, Chen C-C, Lee C-C. Electrically tunable liquid crystal waveguide attenuators. *Opt Express*. 2011;19(12):11890.
68. d'Alessandro A, Martini L, Civita L, Beccherelli R, Asquini R. Liquid crystal waveguide technologies for a new generation of low-power photonic integrated circuits. *SPIE Proc*. 2015;9384:74–81.
69. Zhao H, O'Brien K, Li S, Shepherd RF. Optoelectronically innervated soft prosthetic hand via stretchable optical waveguides. *Sci Robot*. 2016;1(1):Article eaai7529.
70. Wang A, Das A, Grojo D. Ultrafast laser writing deep inside silicon with THz-repetition-rate trains of pulses. *Research*. 2020;2020:Article 8149764.
71. Kollipara PS, Li J, Zheng Y. Optical patterning of two-dimensional materials. *Research*. 2020;2020:Article 6581250.
72. Lin Z, Hong M. Femtosecond laser precision engineering: From micron, submicron, to nanoscale. *Ultrafast Sci*. 2021;2021:Article 9783514.
73. Chen B, Zhao Z, Morris SM. Chiral switches bring new twist to photonics. *Nat Photonics*. 2022;16:174–175.
74. Li L, Lin H, Qiao S, Zou Y, Danto S, Richardson K, Musgraves JD, Lu N, Hu J. Integrated flexible chalcogenide glass photonic devices. *Nat Photonics*. 2014;8:643–649.
75. Salari V, Rodrigues S, Saglamyurek E, Simon C, Oblak D. Are brain–computer interfaces feasible with integrated photonic chips? *Front Neurosci.* 2022;15:780344.
76. Cabrera LY, Weber DJ. Rethinking the ethical priorities for brain–computer interfaces. *Nat Electron*. 2023;6:99–101.
77. Ahmad Tarar A, Mohammad U, Srivastava SK. Wearable skin sensors and their challenges: A review of transdermal, optical, and mechanical sensors. *Biosensors*. 2020;10(6):56.
78. Kuenstler AS, Kim H, Hayward RC. Liquid crystal elastomer waveguide actuators. *Adv Mater*. 2019;31(24):Article e1901216.
79. Batula AM, Mark J, Kim YE, Ayaz H. Developing an optical brain-computer interface for humanoid robot control. In: Schmorrow D, Fidopiastis C, editors. *Foundations of augmented cognition: Neuroergonomics and operational neuroscience. AC 2016. Lecture Notes in Computer Science*. Cham: Springer; 2016.
80. Chen B, Zhao Z, Nourshargh C, He C, Salter PS, Booth MJ, Elston SJ, Morris SM. Laser written stretchable diffractive optic elements in liquid crystal gels. *Crystals*. 2022;12(10):1340.
81. Sandford O'Neill J. 3D switchable diffractive optical elements fabricated with two-photon polymerization. *Adv Opt Mater.* 2022;10(7):2102446.
82. Szobota S, Isacoff EY. Optical control of neuronal activity. *Annu Rev Biophys.* 2010;39:329–348.
83. Boyden ES, Zhang F, Bamberg E, Nagel G, Deisseroth K. Millisecond-timescale, genetically targeted optical control of neural activity. *Nat Neurosci.* 2005;8(9):1263–1268.
84. Xiong H, Alberto KA, Youn J, Taura J, Morstein J, Li X, Wang Y, Trauner D, Slesinger PA, Nielsen SO, et al. Optical control of neuronal activities with photoswitchable nanovesicles. *Nano Res*. 2023;16(1):1033–1041.
85. Ayaz H, Shewokis PA, Bunce S, Onaral B. An optical brain computer interface for environmental control. *Annu Int Conf IEEE Eng Med Biol Soc*. 2011;2011:6327–6330.
86. Tang X, Shen H, Zhao S, Li N, Liu J. Flexible brain–computer interfaces. *Nat Electron*. 2023;6:109–118.